PERGAMON

International Journal of Multiphase Flow 28 (2002) 69–92

International Journal of Multiphase Flow

www.elsevier.com/locate/ijmulflow

Diffusion of spherical bubbles in a turbulent boundary layer

Keith Felton [a], Eric Loth [a,b,*]

[a] *Department of Aeronautical and Astronautical Engineering, University of Illinois at Urbana Champaign, Urbana, IL, USA*

[b] *AAE Department, UIUC, 306 Talbot Laboratory, 104 South Wright Street, Urbana, IL 61801-2935, USA*

Received 13 April 2000; received in revised form 15 August 2001

Abstract

Dilute suspensions of spherical air bubbles in a liquid-turbulent boundary layer were experimentally studied to note the motion and distribution. Bubbles with diameters of 0.37–1.2 mm were injected at various transverse wall positions in upward flowing water of free-stream velocities between 0.4 and 0.9 m/s. Bubble injection frequency was limited to very low mean void fractions, ca. 0.01% in order to avoid bubble coalescing at the wall for certain flow conditions. The experimental diagnostics included bubble tracking for bubble trajectories and planar laser intensity profiles for bubble concentration distribution. Data for the lateral void fraction distributions were collected over a sufficiently long sampling time to allow statistical description of the bubble diffusion.

Three types of bubble motion were observed in the boundary layer: free-dispersing bubbles were drawn to the wall (by transverse fluctuations), bounced along the wall (by coefficients of restitution of order unity), and sliding bubbles along the wall trapped by lift forces. This led to a variety of void profiles: from peaking at the wall to diffusing beyond the mean boundary layer width, depending on the Stokes number and bubble injection location. In general bubbles collected along the wall for high Stokes number conditions (larger bubbles or weaker turbulence). In contrast, the lower Stokes number conditions produced Gaussian-type profiles throughout the boundary layer, which were associated with a tendency for the smaller bubbles to act like tracer particles dispersing throughout the flow. Qualitative measurements of intermediate-size bubbles indicated diffusion rates as a function of drift parameter which were similar to that expected from solid particle diffusion and free shear bubble diffusion.

* Corresponding author. Tel.: +1-217-244-5581; fax: +1-217-244-0720.
E-mail address: e-loth@uiuc.edu (E. Loth).

0301-9322/02/$ - see front matter
PII: S0301-9322(01)00060-X

1. Introduction

The distribution of air bubbles can significantly affect the performance of surface ships, heat exchangers and mixers. As will be discussed, the problem of bubble behavior in gas–liquid flows has been studied extensively for *ellipsoidal* bubbles in internal turbulent flows. Researchers, particularly experimentalists, have shown that void fraction, one of the most used parameters for liquid–bubble interaction, has various distributions. The bubble size and flow conditions were reported as the controlling parameters for the void fraction distributions.

However, there is a limited knowledge as to how turbulence in wall-bounded flows controls void fraction (α) distributions and trajectories for spherical bubbles. The present study sought to experimentally investigate the mechanisms for such aspects in a vertical turbulent boundary layer for various bubble sizes and fluid dynamic conditions. The primary objective of this investigation was measuring various types of void fraction distribution and understanding their development. In the following section, previous studies for three relevant experimental bubbly flow conditions are discussed: free shear flows, pipe flows, and boundary layer flows. Free shear flows are characterized by an entraining fluid that has no direct impact from a fixed boundary on the flow field. In contrast, both boundary layer and pipe flows have flow field structures that are directly impacted by the presence of a solid surface. An essential difference between these two groups is that the boundary layer flow continues to develop and is bounded by a non-turbulent region.

1.1. Bubbles in free shear layers

Similar to investigators of single-phase shear layers, gas–liquid flow researchers have concentrated on coherent eddy structures for insight into the bubble transport. In the limited quantity of bubbly shear-layer studies, researchers have often explored this flow type using numerical analysis rather than experimental techniques.

For example, Tio et al. (1993) numerically studied spherical bubble dispersion in an array of (non-turbulent) Stuart vortices with gravity perpendicular to the streamwise direction. The surface tension of the bubbles was assumed to allow them to act as rigid spherical buoyant particles. Their results demonstrated the importance of the drift parameter $\gamma = V_{\text{term}}/v'$, where V_{term} is the terminal velocity of the bubble in quiescent flow and v' is rms of the velocity fluctuations (and thus related to the turbulence intensity of the surrounding fluid). In particular, bubbles escaped the vortex core for $\gamma \gg 1$, and they remained trapped for $\gamma \ll 1$. Sene et al. (1994) numerically examined the bubble transport in horizontal turbulent shear flows by using a discrete vortex method. They found that bubbles are trapped when γ became less than a critical value and that higher values of γ were associated with decreased diffusion. It should be noted that the drift parameter (γ) for a bubble of negligible density (compared to its surrounding) is proportional to the ratio of Stokes number (St) and eddy Froude number (Fr) as discussed by Loth (1998, 2000). Herein, we define $St = C_{\text{M}} V_{\text{term}} U_0/(g\delta)$ and $Fr = U_0^2/(4g\delta)$, where C_{M} is the particle added mass coefficient (1/2 for a sphere), U_0 is the free stream velocity for a boundary layer (or velocity difference for a shear layer), g is the gravitational constant, and δ is the boundary layer thickness (or shear layer thickness). The local Stokes number is the ratio of bubble response time to local eddy integral time scale and the eddy Froude number is the ratio of hydrodynamic pressure gradients to hydrostatic pressure gradients.

Ford and Loth (2000) recently conducted a series of vertically-oriented mixing layer studies for ellipsoidal bubbles. They noted increased void spreading as the flow speed was increased for a given bubble diameter size, owing to higher turbulence mixing for the higher liquid velocity. This was attributed to a lower γ, which allowed for longer bubble–eddy interaction times, resulting in increased turbulent diffusion. These results are consistent with Eulerian model of solid-particle diffusion by Stock (1996) and Loth (2000) which indicate particle diffusion is similar to that for a scalar for $\gamma \ll 1$, and then monotonically decreases as γ increases. An increase in Stokes number yields a similar phenomenon but with the added complexity that a range of eddy Froude numbers yields a family of diffusion curves.

1.2. Bubbles in pipe flows

Numerous experimental studies have been conducted for bubbles in pipe flows, where generally experimentalists have sought to document and understand void profiles. Results from upward-flowing, pipe flows show three types of void fraction profiles: "coring" or "core-peaking" (Nakoryakov et al., 1981; van der Welle, 1985; Beyerlein et al., 1985), "wall-peaking" (Serizawa et al., 1975; Beyerlein et al., 1985; Michiyosi et al., 1986; Wang et al., 1987; Liu, 1993) and "saddle" profiles (Sekoguchi et al., 1981; Wang et al., 1987). Coring void profiles are associated with a high percentage of bubbles along the pipe centerline, while wall peaking profiles have a predominance of bubbles along the pipe wall. Saddle profiles have a nearly equal quantity of bubbles along the wall and pipe centerline. Serizawa et al. (1975) noted that the various bubble size distributions governed the type of void fraction profile – wall-peaking, coring, and saddling. Most internal flow studies have shown that the smaller ellipsoidal bubbles migrate toward the outer wall whereas larger bubbles transport along the core. The bubble diameter (d_B) distribution is also strongly influenced by the liquid velocity and void fraction, where higher liquid velocity conditions produce stronger turbulent mixing which presumably lifts bubbles off the wall often producing a coring profile.

There is substantial debate as to the exact cause of wall-peaking, i.e. whether it is a product of the turbulence gradients, bubble lift forces, weak pressure gradients, bubble sizes, eddy dynamics, or a combination of these factors. This debate is complicated by the fact that most of the experiments have included significant polydispersion of bubble size and non-dilute conditions (i.e. $\alpha > 1\%$) where significant bubble–bubble interaction and turbulence modulation can occur (both of which can lead to significant modification of the bubble distribution).

In addition, all of these studies only investigated ellipsoidal bubbles (e.g. $d_B > 1.2$ mm for air in water). This presents another substantial limitation to understanding spherical bubble dispersion, since ellipsoidal bubble shapes introduce a significant trajectory oscillation, an entire family of drag coefficient curves, and even lift reversal (Ford and Loth, 1998).

To allow more direct insight into the bubble motion in wall-bounded turbulent flows, researchers have recently shifted attention to the flat plate boundary-layers where the presence of a non-turbulent far-field can simplify the underlying interactions. Similar to the bubbly pipe flows, the research of bubbles in flat-plate turbulent flows can be generally divided based on the bubble diameter shape: ellipsoidal bubbles and spherical bubbles. Since the former is more common, it is discussed first.

Experimental investigations of deformable, non-spherical bubbles in liquid turbulent boundary layers along a flat plate include Moursali et al. (1995), Lance and Bataille (1991), and Tran-Cong et al. (1997). These studies experimentally explored void fraction distribution, wall interaction, and diffusion mechanisms for deformable bubbles in a vertical turbulent boundary layer. Essentially, they examine *quantitatively* many of the issues that will be explored in the present spherical bubble study. Moursali et al. (1995) conducted one of the few void fraction distributions studies for a mono-disperse boundary-layer flow, where bubbles with a mean diameter of 3.5 mm were introduced near the leading edge of the flat plate. The void fraction was approximately 1.5%, constituting a nearly dilute flow. They observed the flow field with a CCD camera and measured the void fraction with an optical probe located 1 m down stream of the leading edge. The results show significant wall-peaking of the void fraction, where the peak tends to occur at a transverse position somewhat greater than the bubble radius ($Y_{\text{peak}}/d_{\text{B}} \sim 0.65$). When the bubble size distribution broadened to primarily include larger sizes at higher void fractions, the relative wall-peaking was significantly reduced in intensity as more bubbles appeared in parts of the flow away from the wall. This result is qualitatively consistent with pipe flow measurements described above (i.e. larger bubbles tended to produce void peaks at the pipe centerline). Recent measurements of ellipsoidal bubble trajectories by Tran-Cong et al. (1997) indicate that smaller bubbles migrate more toward the boundary-layer plate and then become trapped inside the boundary layer (i.e. they do not escape).

Investigations of *spherical* bubble diffusion in boundary layers are quite scarce. Merkle and Deutsch (1992) have conducted one of the few spherical bubble investigations for flat plate bubble flows. They studied the effectiveness of introducing a high concentration of very small bubbles (i.e. micro-bubbles) along a horizontal plate for use as a drag reduction mechanism. Merkle and Deutsch (1992) noted that the micro-bubbles tended to diffuse throughout the turbulent boundary layer. However, the information on bubble trajectories and diffusion way only qualitative, since the focus was primarily on the resulting skin friction reduction and the bubble sizes were highly poly-disperse with only a rough approximation of the mean diameter given. As such, no turbulent internal flow study (boundary layers or pipe flows) has measured detailed mean void fraction profiles or individual bubble trajectories for spherical mono-disperse bubbles. This investigation seeks to investigate these areas for a range of flow speeds, injection locations and bubble sizes.

2. Experimental methods

2.1. Flow facility

The dynamics of millimetric air-bubbles inside a vertical, wall-bounded liquid shear layer were experimentally investigated in this study. The experimental facility is located in the UIUC Hydrosystems Laboratory and consists of a closed loop water tunnel. The tunnel volume is approximately 4500 l, with a passive bubble trap located at the top of the water tunnel to eliminate bubble recirculation. In the water tunnel test section, a boundary layer plate and a bubble injection system were installed (Fig. 1). Details of the set-up may be found in Felton (1999) and Felton and Loth (2001). The spanwise width and depth of the test region are 30 cm each, providing sufficient spanwise and transverse distance to ensure negligible wall effects in the test interrogation region.

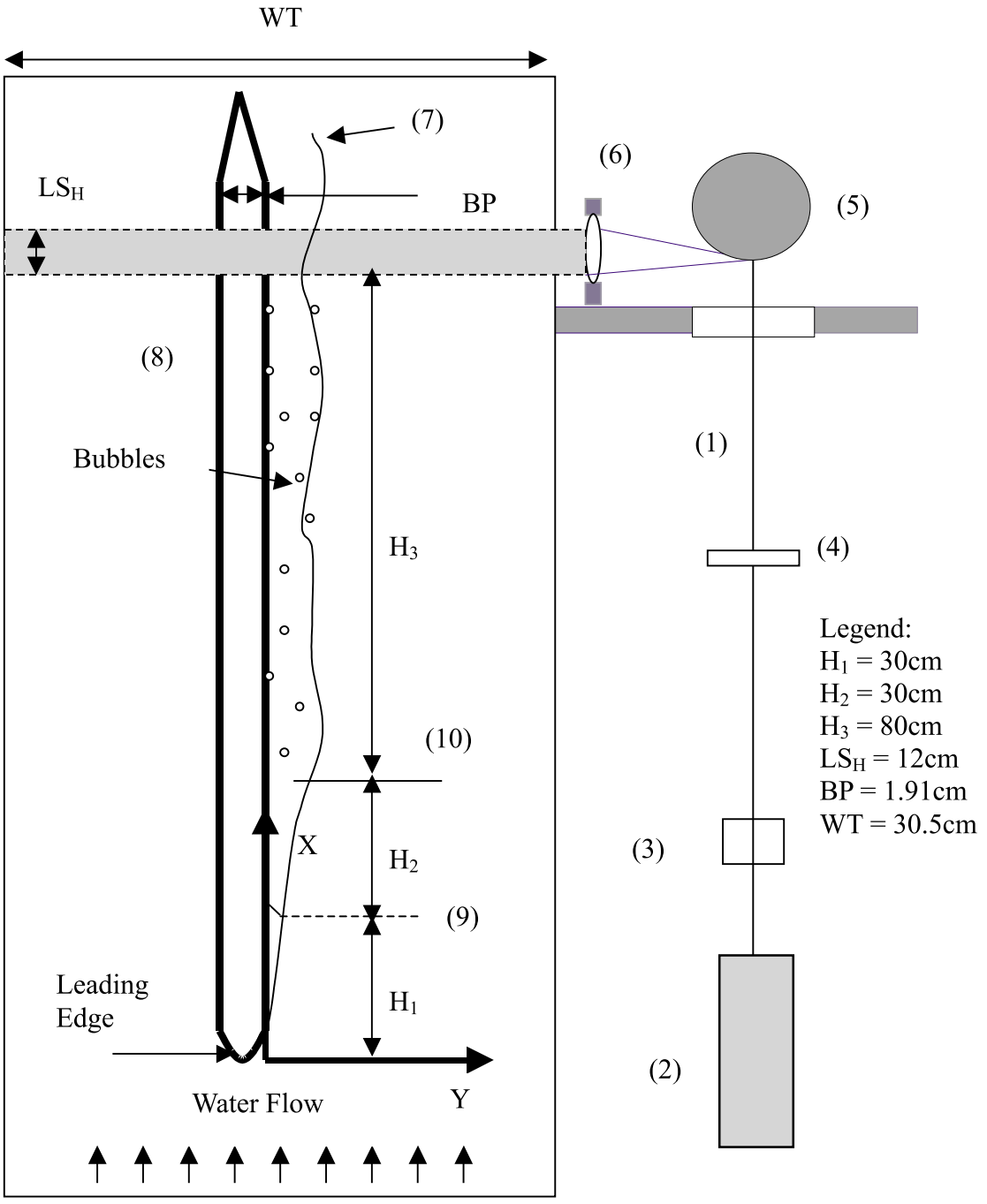

Fig. 1. Schematic of boundary layer plate and optical arrangement of the laser sheet with respect to field of view. The incoming beam (1) for the laser sheet projection is produced via a 5W Argon-Ion laser (2), beam directing mirror (3), focusing lens (4), 24-sided scanning mirror (5), and collimating lens (6). The turbulent boundary layer (7) is established by the boundary layer plate (8) and tripping mechanism (9). The bubble injector (10) could be traversed horizontally (normal to the boundary layer plate).

Table 1
Summary of key results for bubble concentration distributions

Test run #	St ($\times 10^2$)	Fr ($\times 10^2$)	V_{term}/v'	Y_{peak}/δ	Y_{peak}/d_B	Y_{peak}/Y_{inj}	σ/δ	Distribution profile
2	5.6	12	7.3	0.020	0.83	0.050	–	I
19	5.6	12	7.3	0.015	0.62	0.043	–	I
3	3.0	12	5.1	0.870	63.80	1.088	0.6	III
4	5.6	12	9.5	0.013	0.54	0.016	–	II
5	8.2	12	13.5	0.019	0.52	0.024	–	I
6	4.3	33	1.9	0.500	37.84	1.250	1.1	III
7	8.6	33	4.2	0.010	0.40	0.025	–	I
8	12.2	33	6.0	0.020	0.56	0.050	–	I
12	3.0	12	4.0	0.460	33.73	1.150	0.55	III
2	5.6	12	7.3	0.020	0.83	0.050	–	I
19	5.6	12	7.3	0.015	0.62	0.043	–	I
2	5.6	12	7.3	0.020	0.83	0.050	–	I
15	5.6	12	8.4	0.020	0.83	0.033	–	II
4	5.6	12	9.5	0.013	0.54	0.016	–	II
9	5.6	12	19.0	1.290	53.21	1.075	0.25	IV
6	4.3	33	1.9	0.500	37.84	1.250	1.1	III
10	4.3	33	2.5	0.850	64.32	1.063	0.7	III
11	4.3	33	5.0	1.280	96.86	1.067	0.3	IV
13	8.2	12	9.6	0.027	0.74	0.225	–	I
5	8.2	12	13.5	0.019	0.52	0.024	–	I
7	8.6	33	4.2	0.010	0.40	0.025	–	I
17	8.6	33	4.9	0.027	1.08	0.045	–	II
18	8.6	33	5.5	0.017	0.68	0.021	–	II
5	8.2	12	13.5	0.019	0.52	0.024	–	I
18	8.6	33	5.5	0.017	0.68	0.021	–	II

The flow field's boundary layer was produced as a result of the upward flowing wall-bounded liquid at velocities from 0.4 to 0.9 m/s, and the resulting flow conditions are listed in Table 1.

The present turbulent boundary layer was artificially produced using a tripping device, which consisted of a series of spanwise delta wings fixed to the plate and set at angle of attack to the incoming flow. The resulting delta wings, at a height of approximately 4 mm, were located 30 cm downstream of the leading edge. This streamwise location and tripping device height were selected to ensure that fully turbulent flow conditions began immediately downstream of the roughness location, per the method of Braslow et al. (1996).

The tap water in the tunnel was filtered (prior to seeding with PIV tracers) through filter papers with a 2.5 μm pore size. This filtration was necessary to eliminate any particulates with a diameter on the order of the seeding particle size of 8 μm. No other water treatment was employed, such that the immobilization of the liquid–gas interface caused by natural contaminants is expected to be approximately consistent with other "tap water" experiments.

2.2. Bubble generation system

The bubble generation system is shown in Figs. 1 and 2. It consisted of a 0.005 l syringe tube, a hypodermic needle, a syringe pump, an EFT valve, and a compressed air tank based on the single-bubble injection technique of Park et al. (1995). However, the present set-up differs in that an additional pressure line was added to the syringe to allow multiple injections without draining the water tunnel. The compressed air was delivered through the hypodermic needle with various injection tip sizes (22, 26, 28, 30 and 32 gauge) to produce mono-disperse bubble diameters of 370–1200 μm inside the turbulent boundary layer.

A high precision Cole Parmer (model E 74900-00) syringe pump with a rated accuracy of ±0.5% was used to produce the air for the bubbles. An air-flow rate of 2–3 ml/h was employed to ensure low mean void fractions (ca. 3×10^{-5}) in the boundary layer test region such that both bubble–bubble interactions and turbulence modulation were negligible for all conditions.

Bubbles were injected over a range of transverse (i.e. horizontal) positions conditions. This transverse bubble injection location (Y_{inj}/δ) varied over a range of 0.1–1.2, where δ is the field-of-view boundary layer thickness. The vertical injector exit position was located 80 cm upstream of the laser field of view. Since air bubbles in water achieve their terminal velocity in less than a centimeter, the injector location assured that the bubble motion in the field of view was essentially independent of their formation at the injector and the location allowed significant diffusion to

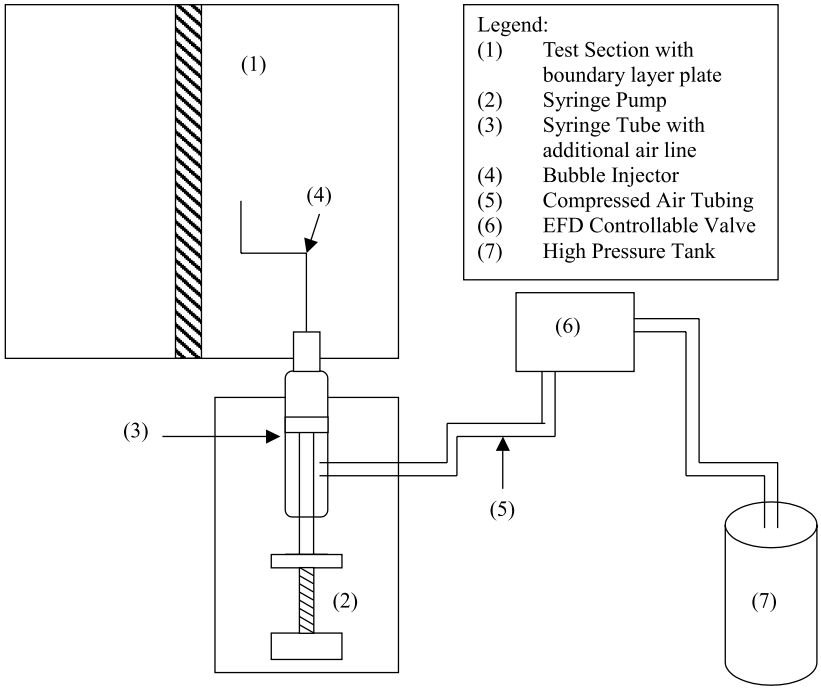

Fig. 2. Schematic of bubble injection system used to produce mono-disperse bubbles, where test section cross-section (perpendicular to flow) is shown.

occur. In addition, the wake of the thin 0.72 mm OD injector tube is expected to have a negligible impact on the downstream boundary layer development and structure.

Bubble sizing for each test condition was conducted with a high-magnification camera, which was validated with spherical glass beads (0.3–1.0 mm) temporarily adhered to the boundary layer plate in the test section. For quiescent flow, bubble diameters were consistent with the bubble release volume estimates of Oguz and Prosperetti (1993), but were reduced as the upward liquid velocity increased. The maximum diameter uncertainty was 3.6% and the maximum standard deviation for the diameter distributions was ±4.7%.

2.3. Bubble distribution technique

Measurements of the bubble population concentration were obtained using a laser intensity methodology (Ford and Loth, 2000). The technique employed a Spectra-Physics 5W Argon-Ion Laser, 24-sided Lincoln Laser rotating mirror, and various lens and mirrors designed to steer and focus the laser beam (see Fig. 1). The rotating mirror has a variable frequency range of 5–50 Hz, and it is coated with an Al–SiO reflective coating with a surface flatness of 1/4 wavelength. Precise machining, and assembly ensured that the mirror surfaces are parallel to the rotating axis, which is critical to produce identical laser scanning sheets. The rotating mirror frequency was set to produce four sweeps for each film frame. Following the rotating mirror is a 145 mm diameter collimating lens with a 250 mm focal length. It is designed to produce a beam sweep of 122 mm. A measurement and estimate of the beam thickness shows a 1 mm thick beam is projected into the interrogation region. This method allows one to record individual bubbles as they move through the test interrogation region by tracking its location at every laser sweep. The tracking of several hundred bubbles over a long time period for each condition yielded statistically sufficient bubble population distribution measurements.

The images of the bubble trajectories in the test interrogation region were acquired using a 35 mm Canon T-90 camera equipped with a 100 mm $f^{\#}$ 4.5 macro lens, 12 mm extension tube and a 60 second shutter speed (i.e. sampling time) for observing the bubble distribution. Twenty-five to thirty photographs were recorded for each test condition, yielding a total sample time of 25–30 min per test run and the net acquisition of thousands of bubble images. the film negatives were digitized using the high resolution (800 ppi) Studio scanner II. A scanned background photograph (with no bubbles) was subtracted from each bubbly flow photograph, which were then thresholded. An example image is given in Fig. 3, which shows a dozen or so bubbles that are scanned at several points of their trajectory by the laser and rotating mirror system.

The 25 resulting digital images for each test condition were ensemble-averaged and row-averaged to determine the intensity along pixel columns normal to the boundary layer. Each row represented the transverse bubble concentration for a discrete streamwise position in the laser sheet. The resulting distribution was equated to the local bubble number concentration, which in turn is proportional to the void fraction distribution (α) for monodisperse bubbles. Generally, the void fraction peak ($\alpha/\alpha_{max} = 1$) was found to be reproduceable within 5% of δ (and within 2% of δ when the peak was near the wall). This image intensity method was validated with a bin method

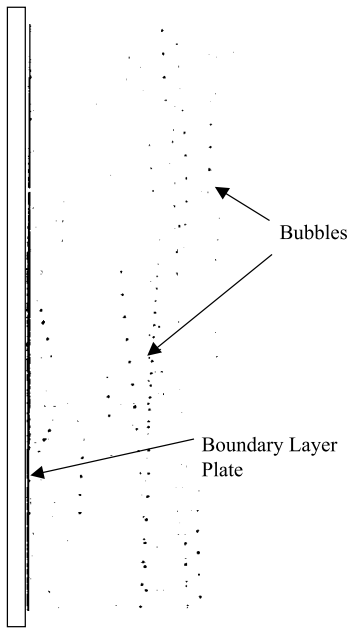

Fig. 3. A sample scanned image of bubbles dispersing inside the boundary layer. This image is typical for a 25-s interval.

where all individual bubble images were counted to alternatively obtain the mean bubble number distribution; the comparison indicated a void peak location uncertainty for the image intensity method of less than 5% of δ. The orientation of the horizontal bubble injector was varied to note its potential influence. The results for the injector pointing towards the wall versus pointed in the spanwise direction indicated negligible differences, such that the initial bubble velocity was not important to the test section void distribution.

3. Results

3.1. Single-phase flow field

Three free stream velocities ($U_0 = 0.4$, 0.6, 0.9 m/s) were employed in this study and investigated with a PIV system (Felton and Loth, 2001). The PIV system was used to study both the single and two-phase flow conditions, and for the present flow conditions the differences in the mean statistics were insignificant, indicating negligible turbulence modulation. The streamwise distribution was also found to be in accordance with previous low Reynolds flat-plate turbulent boundary layers studies (Meinhart, 1994; Tomkins, 1997; Klebanoff, 1954), indicating the conventional tripping device performed as expected even for the lowest flow speed. In addition, the transverse velocity profile normalized by the freestream is less than 2% for $0.0 < y/\delta < 1.0$. Further details are given in Felton and Loth (2001).

3.2. Void fraction profiles

A summary of the major test parameters and resulting void fraction profiles are tabulated in Table 1. For the test conditions of the present study, four distinct bubble distribution profiles were identified, and they are classified as Type I, Type II, Type III, and Type IV profiles. These profiles are given schematically in Fig. 4(a). Type I profiles resulted in almost all bubbles trapped along the wall (with little or no bubble drift away from the wall). Type II profiles exhibited a high concentration of bubbles trapped along the wall (similar to Type I), but also included a significant portion of bubbles dispersing away from the wall. Type III profiles exhibited bubble dispersion throughout the boundary layer with a concentration peak near the transverse injection point. Type IV profiles yielded bubble trajectories primarily along the mean boundary layer edge. Of the four, the Type III void fraction profiles tended to cover the largest fraction of the boundary layer thickness and were characterized by a Gaussian type transverse distribution. Note that the Types I, II, and III profiles are, respectively, similar to the "core-peaking", "saddle" profiles, and "wall-peaking" distributions for pipe flows. Whereas the Types I and III profiles are, respectively, similar to the Moursali et al. (1995) "wall-peaking" and Merkle and Deutsch (1992) boundary layer diffusion. The Type II bi-modal profile (previously unreported for boundary layer flows)

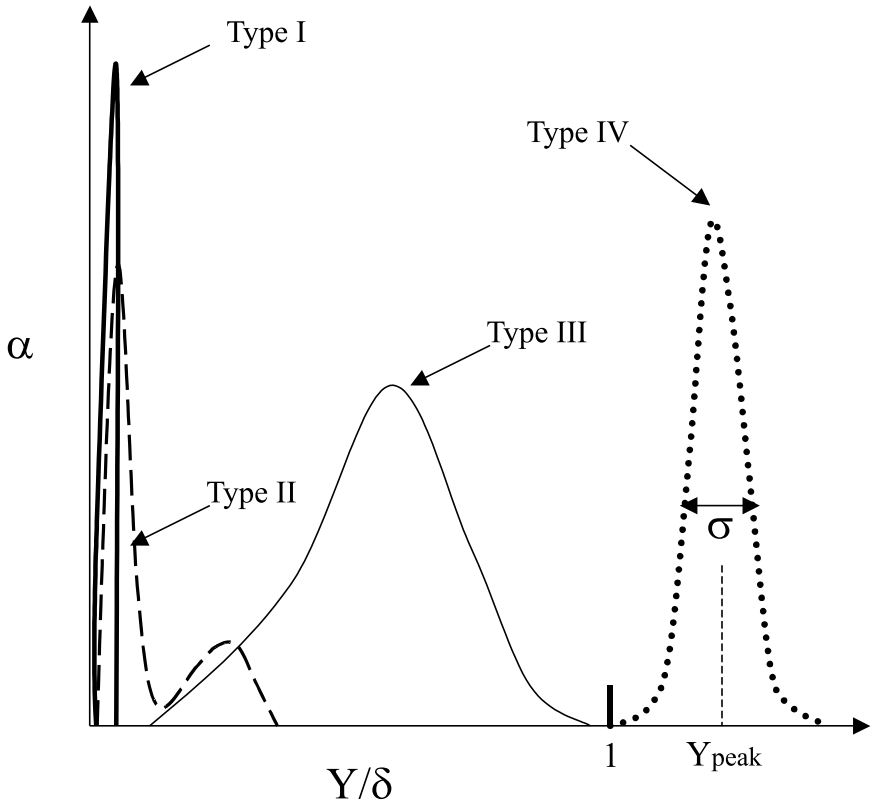

Fig. 4. Schematic of observed void distribution profiles, with void peak location and void width shown for the Type IV profile. Note δ is defined at the void measurement region (not at the bubble injection point).

indicates that lift and drag forces can selectively segregate significant mono-disperse bubble populations injected from a single location. The Type IV profile also indicates that significant diffusion without large entrainment can occur and remain just at the outside edge of the boundary layer. A description of how these individual profiles tend to occur is given later (in the discussion of individual bubble trajectories).

Figs. 5 and 6 depict examples of the influence of Stokes number while holding the Fr_δ and Y_{inj}/δ constant (further results are available in Felton, 1999). Fig. 5 gives concentration measurements for the lowest-speed flow case showing three of the four distribution types for relatively modest variation in St for 0.03 to 0.12. The trend of spherical bubbles exhibiting a free-dispersion trajectory at low Stokes number found in Fig. 5 is also found in Fig. 6. However, the Type I behavior occurred at a larger St in Fig. 6 which was attributed to the smaller injection location $Y_{inj}/\delta = 0.4$, indicating that the combination of St and Y_{inj}/δ are important in determining void distribution type. As Stokes number (and γ) are increased due to a larger bubble diameter, one witnesses a transition from bubble diffusion throughout the boundary layer to bubbles collecting along the wall. These results are consistent with the Merke and Duetch (1992) boundary layer diffusion for smaller bubbles and the Moursali et al. (1995) "wall-peaking" for larger bubbles. Though bubbles are injected a relatively large distance away from the plate ($Y_{inj}\delta = 0.8$), the highest Stokes number

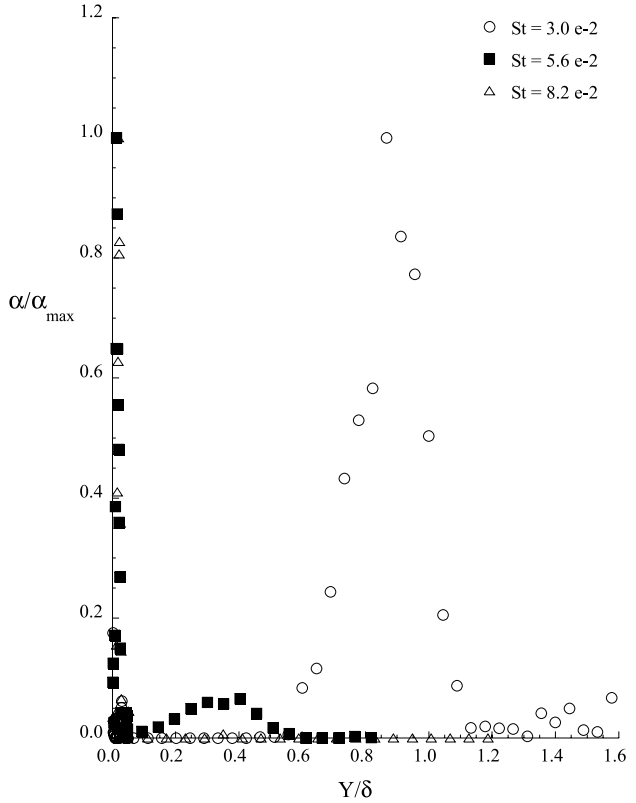

Fig. 5. Bubble concentration distribution for fixed Fr (12e − 2), Re_δ (13e3), and $Y_{inj}/\delta(0.8)$ values and varying St number (3.0e − 2 to 8.2e − 2).

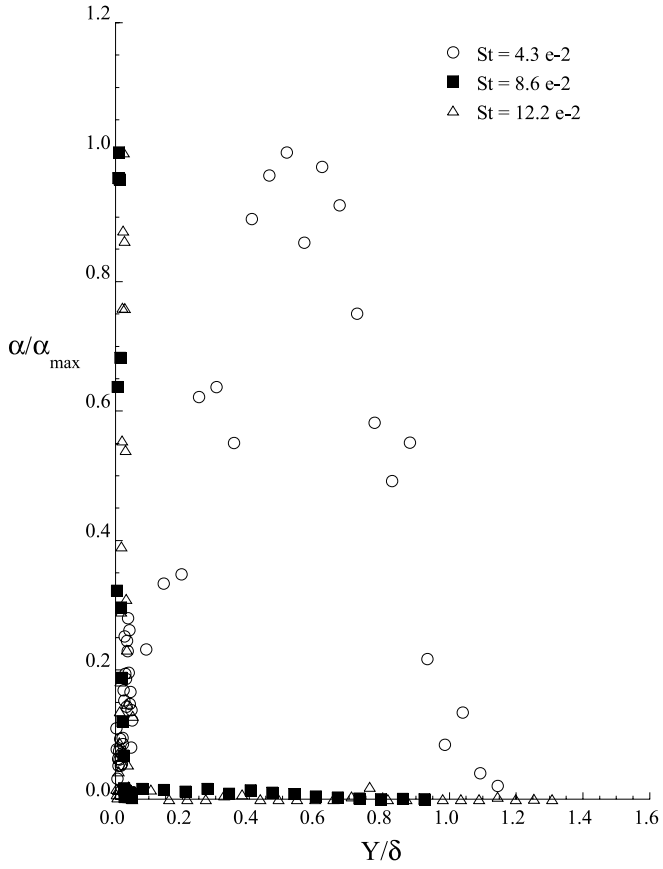

Fig. 6. Bubble concentration distribution for fixed *Fr* (33e − 2), Re_δ (16e3), and $Y_{inj}/\delta(0.4)$ and varying *St* (4.3e − 2 to 12.2e − 2).

condition (0.082) resulted in bubbles primarily trapped along the wall, i.e. Type I behavior. Once the bubbles are near the wall, they can be retained through lift forces, as demonstrated by the measurements of Felton and Loth (2001).

The wall-peaking effect is consistent with results for solid particle flow studies (Young and Hanratty, 1991; Loth, 1998) whereby the lift forces (based on mean terminal velocity and mean boundary layer shear) are in the direction of the wall. However, this trend is opposite to that noted for ellipsoidal bubbles in an external turbulent boundary layer (Tran-Cong et al., 1997); the difference may be related to the bubble deformation which can cause reversal of the lift direction (Ford and Loth, 1998).

Figs. 7–9 show the influence of holding the *Fr* and *St* constant and varying Y_{inj}/δ. Generally, the profiles proceed from Types I to IV as Y_{inj}/δ is increased. Comparison of Figs. 8 and 9, which have the same Froude number but different Stokes numbers (0.086 and 0.043), indicates that the injection location trend toward Type IV is substantially accelerated as *St* (and γ) is decreased by a factor of two. Fig. 10 depicts the influence of varying *Fr* and γ while holding the Stokes number

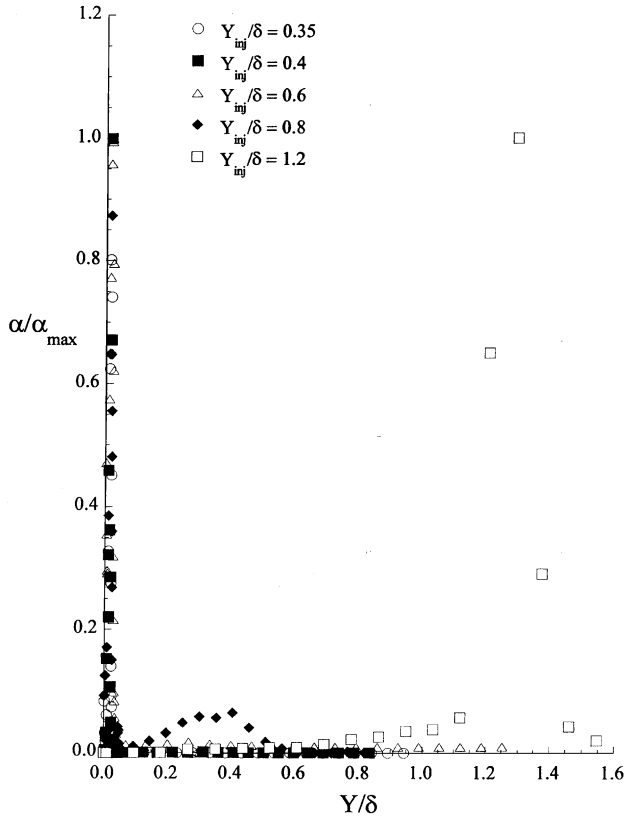

Fig. 7. Bubble concentration distribution for fixed Fr (12e − 2), Re_δ (13e3), and St (5.6e − 2) and varying Y_{inj}/δ values (0.35 to 1.2).

constant. The lower γ value exhibited more diffusion, which is again consistent with turbulent dispersion of free-shear particles, as will be discussed in the next section. In general, the net transverse bubble distribution thicknesses were a small fraction of the total streamwise diffusion length (e.g. 1%), which is consistent with the growth rate of the turbulent boundary layer velocity profile in that same streamwise section.

3.3. Void peak location and void spread rate

The type of void profile distribution which occurred tended to correlate best with the bubble Strokes number and injector location (Felton, 1999). When the four void distribution profiles are compared with Stokes number and the bubble injection location, four parameter regions containing similar profiles are formed (Fig. 11). Low Stokes number and injection values less than δ generally produced Type III profiles (peaks inside the boundary layer with few bubbles near the wall). Higher Stokes number conditions yielded Type I (where most of the bubbles collect along the wall) when injected within $\delta/2$. Type II profiles (wall peaking and secondary peaking away

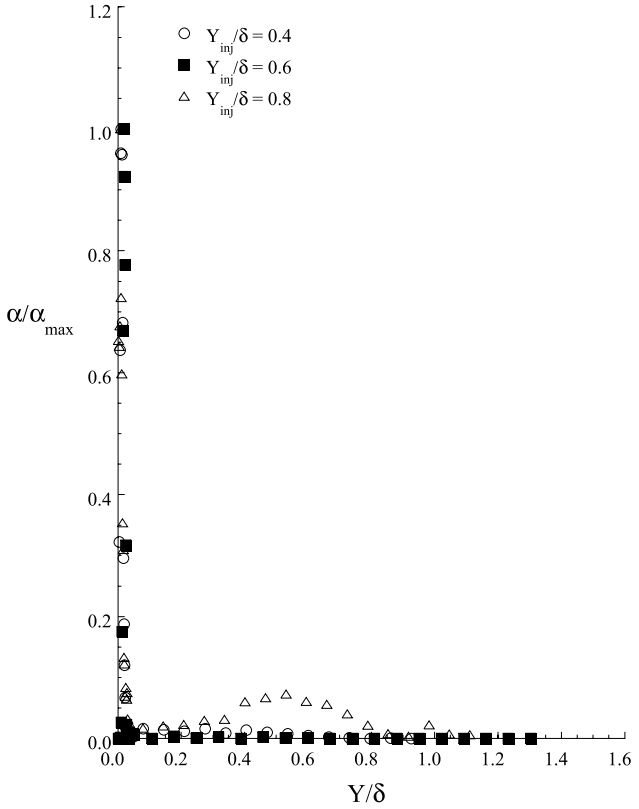

Fig. 8. Bubble concentration distribution for fixed Fr (33e − 2), Re_δ (16e3), and St (8.6e − 2) and varying Y_{inj}/δ values (0.4–0.8).

from the wall) occurred when similarly sized bubbles were injected between $\delta/2$ and δ. However, at least one case in this region was a Type I profile, and the pair of Type II profiles for a non-dimensional injection location of 0.6 indicated very modest secondary peaks (e.g. the profile in Fig. 6). As such, Type I profiles were noted to occur at injection locations up to δ. For bubbles introduced at a transverse position greater than the boundary layer thickness, the resulting profiles are primarily Type IV (peaking beyond δ).

In order to further characterize the void distribution, the concentration peaks and transverse widths (shown in Fig. 4(a)) were obtained. Fig. 12 quantifies the void peak locations for all four types of profiles. From this figure, one can observe that the void peak (Y_{peak}/δ) and the dimensionless bubble injection (Y_{inj}/δ) are approximately equal for Types III and IV profiles. The reason for this behavior is that the mean drift of the bubble cloud toward the wall for $y/\delta > 0.4$ is negligible. This is consistent with the lower mean vorticity in this region, such that lift does not play a significant role in the mean trajectories. Fig. 12 also shows that the Types I and II void peak locations are very small and essentially independent of the Y_{inj}/δ value. These are cases where most of the bubbles collect along the wall. This trend of the larger bubbles collecting along the wall is also consistent with a numerical pipe flow study of 1–2 mm diameter bubbles by Beyerlein

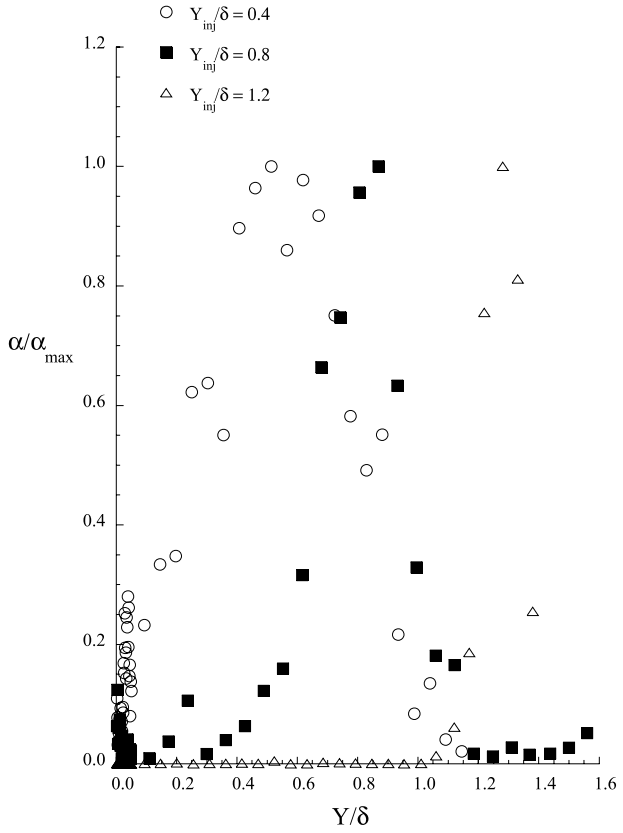

Fig. 9. Bubble concentration distribution for fixed Fr (33e − 2), Re_δ (17e3), and St (4.3e − 2) and varying Y_{inj}/δ values (0.4–1.2).

et al. (1985). Analysis of individual bubble transverse velocities by Felton and Loth (2001) indicates they are too high to be caused by drag but were consistent with the shear-induced lift forces observed by Shridar and Katz (1995).

Fig. 13 provides further insight into the scaling of these near-wall void peak locations with respect to bubble size. Similar to previous ellipsoidal bubble investigations by Serizawa et al. (1975) for pipe flow and Marie et al. (1997) for a flat plate, the peak for the present study is located somewhat more than a mean bubble radius away from the wall ($Y_{\text{peak}}/d_{\text{B}} \sim 0.67$). This suggests that a thin layer of fluid exists on-average between the wall and bubble as it slides along the plate. This result is also qualitatively consistent with experiments for 100 μm glass particles "trapped" at $Y_{\text{peak}}/d \sim 0.65$–$0.87$ in a water pipe flow of Reynolds numbers ranging from 12,700 to 18,700 by Young and Hanratty (1991). The latter study proposed that this trapping phenomenon was caused by a balance of the wall displacement force and the Saffman lift force, although they predicted equilibrium at much closer locations of $Y_{\text{peak}}/d \sim 0.52$–$0.56$.

To gain insight into turbulent diffusion for the bubbles which primarily experience free dispersion, the bubble spread rate of the Types III and IV profiles were considered by measuring the

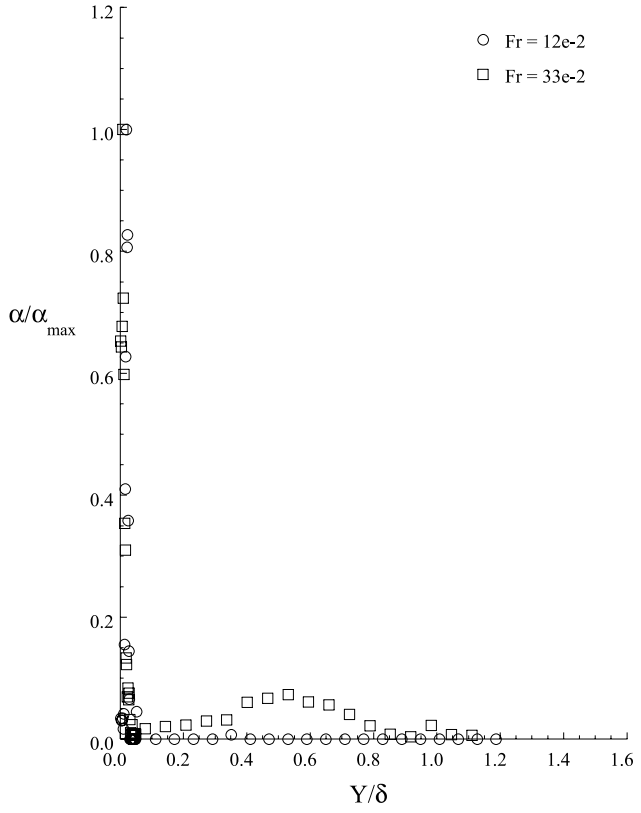

Fig. 10. Bubble concentration distribution for fixed St (8.4e − 2) and Y_{inj}/δ (0.8), and varying Fr (12e − 2 to 33e − 2).

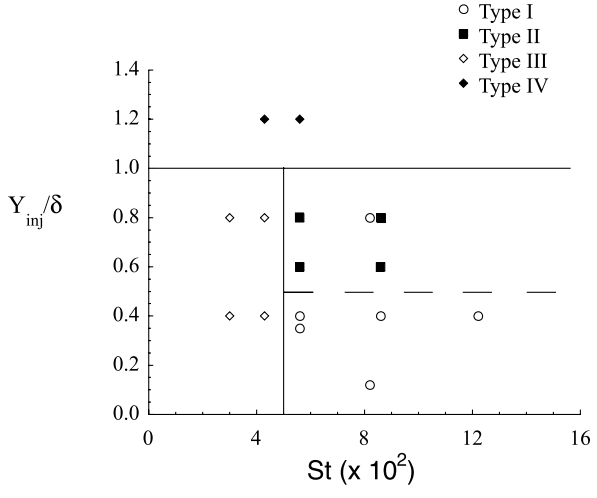

Fig. 11. Comparison of non-dimensional injection points (Y_{inj}/δ) versus Stokes number for the four distribution profiles. Note the Type II profiles at injection location of 0.6 included only small bubble populations away from the wall, i.e. they were only marginally different than typical Type I profiles. Therefore, only a dashed line separates the Types I and II profiles.

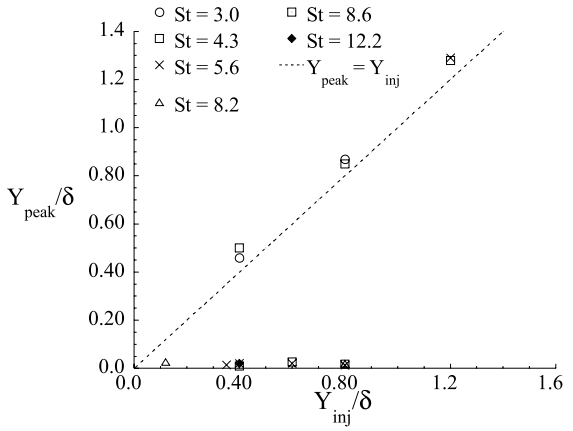

Fig. 12. Comparison of the peak bubble-concentration location versus the bubble injection location, both scaled by the boundary layer thickness at the measuring field (δ).

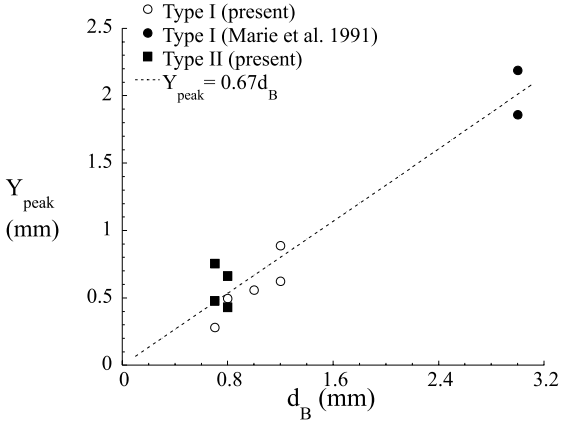

Fig. 13. Comparison of transverse void-peak location for Types I and II profiles with Marie et al. (1997).

transverse width of the void fraction profile (σ). This width was obtained by fitting a Gaussian profile to individual void distribution profiles and measuring the width based whereby the void fraction is 10% of the maximum value, as described by Ford and Loth (2000). The result is primarily qualitative as the uncertainty level for the measured width is of the order of 25%. Felton (1999) compared σ/δ versus both St and γ, and found that the latter provided a more consistent correlation. Note that the values for γ ($= V_{\text{term}}/v'$) are shown in Table 1 and were obtained by extracting the mean transverse turbulence value at the equivalent injection location using the v'_{F} profiles from Felton and Loth (2001). Fig. 14 indicates that the bubble distribution width (σ) decreases as the drift parameter increases, which is qualitatively consistent with results for transverse particle dispersion in homogeneous isotropic turbulence (Reeks, 1977; Stock, 1996; Loth, 2000).

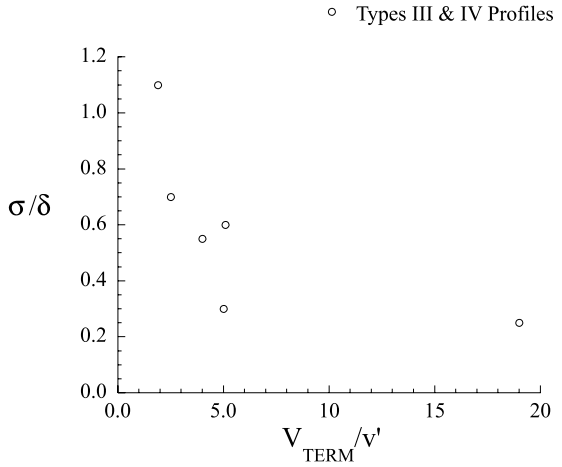

Fig. 14. Bubble diffusion rate as a function of drift parameter number for Types III and IV profiles.

To investigate the approximate diffusion rate, D (the ratio of particle diffusion to scalar diffusion), Felton (1999) converted the present data as per Ford and Loth (2000). The results in Fig. 15 indicate a reduction in transverse diffusion (D) as γ increases similar to the results from a solid particle Eulerian diffusion model (Loth, 2000), whereby D is proportional to $(1 + c\gamma^2)^{-1/2}$, where c is an empirical constant. In addition, the present results qualitatively agree with various bubble data: experiments in a jet flow by Lasheras (1998), experiments in grid-generated turbulence by Poorte (1998), and simulations for homogeneous isotropic turbulence by Bocksell and Loth (1999). This demonstrates that for very small bubbles, one may expect their transverse diffusion to mimic that of a fluid scalar whereas larger bubbles (or weaker turbulence) result in reduced void

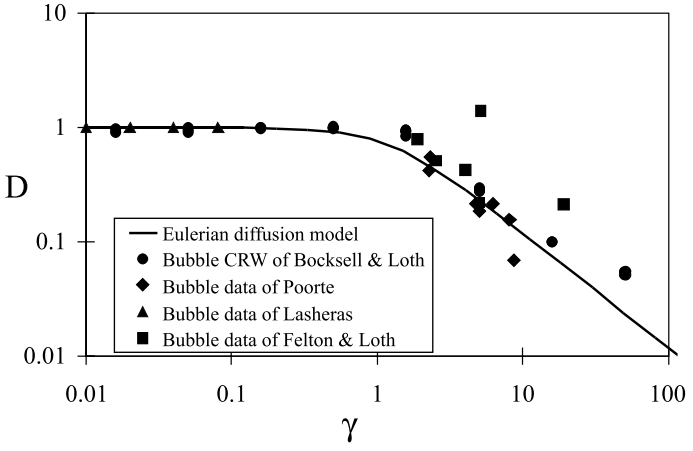

Fig. 15. Comparison of Csanady-based Eulerian diffusion model (Loth, 2000) and other bubble diffusion results with an approximation of present data.

diffusion. The above results are also consistent with the study of spherical solid-particles in dilute pipe flow conditions by Young and Hanratty (1991), whereby heavier steel particles tended to diffuse less than lighter glass particles (consistent with less diffusion as γ increases).

3.4. Bubble trajectories

By analyzing the bubble trajectories individually, three highly distinguishable trajectories were observed: (a) bubbles sliding along the wall, (b) bubbles bouncing along the wall, and (c) bubbles freely dispersing in the boundary layer. The three types are shown with sample trajectories in Fig. 16 and Table 2, where the bouncing bubbles typically became trapped along the wall further

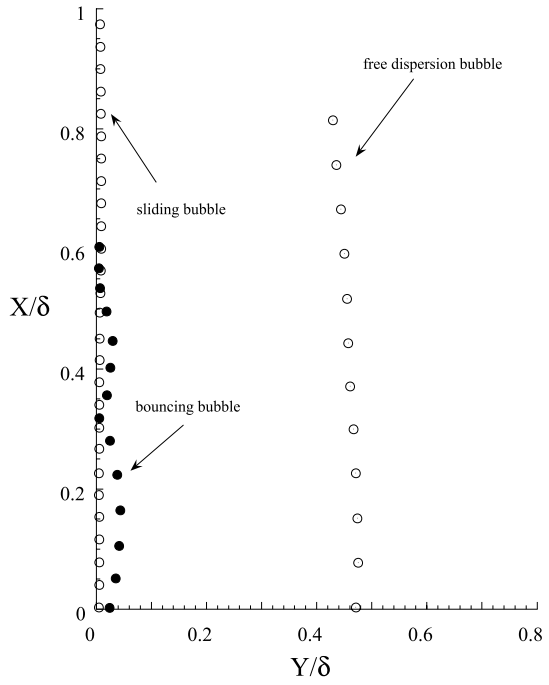

Fig. 16. Sample of millimetric bubble trajectories observed inside the vertical liquid turbulent boundary layer. Three distinct trajectories were observed: (a) free dispersion bubble, (b) bubble bounce, and (c) bubble slide.

Table 2
Category of bubble trajectories

d_B (mm)	Slide	Bounce	Free dispersion
$1.2 < d_B < 0.8$	Yes	Yes	Yes
$0.8 < d_B < 0.6$	Yes	No	Yes
$0.35 < d_B < 0.6$	No	No	Yes

downstream and where the low frequency eddies in the outer region can cause a single bubble to experience a free dispersion effect similar to that found in unbounded shear layers. One of the dramatic differences between the trajectories of various bubble sizes is that the motion of smaller bubbles ($d_B < 0.6$ mm) was primarily limited to free dispersion. Conversely, the large bubbles ($d_B > 0.8$) exhibited all of the observed bubble trajectories – slide, bounce, and free dispersion. This is consistent with wall void-peaking noted primarily for the larger bubbles. All of the trajectories demonstrated that the mean flow has limited impact on the bounce, slide or free dispersion profile. The dominant influence comes from the turbulence intensity and bubbles relative velocity.

For bubbles which eventually migrated toward the wall (i.e. were "trapped"), the typical sequence of events based on the bubble trajectories was as follows: (1) starting from injection, bubbles would disperse laterally in the turbulent boundary layer until a turbulent motion caused them to move quickly toward the wall; (2) at the point of initial impact, the bubbles would typically bounce away from the wall with a coefficient of restitution of approximately 0.8–0.9 for the first few bounces (to be discussed later); (3) after several bounces the bubbles would eventually slide (else they were ejected back into the boundary layer); and (4) the bubbles would then generally slide for a long period and were ejected only occasionally – this ejection either resulted in a new set of bounces or allowed the bubbles to be ejected completely from the near-wall area. The typical stream-wise distance between bounces was of the order of 10 mm (i.e. significantly less than δ), with an increase as the bubble diameter decreased (Felton, 1999). This further suggests that the larger bubbles were more attracted to the wall. As such, this complex trajectory phenomena is related to the turbulent structures and not the mean transverse fluid velocity field. The sliding phenomena and the resulting "wall-peaking" profiles are attributed to the strong lift forces which occur near the wall based on the local velocity shear and the high lift coefficients measured for bubbles of this size (Shridar and Katz, 1995; Felton and Loth, 1999).

The mean relative velocities of the bubbles were also compared to the surrounding fluid and the quiescent rise velocities in Fig. 17. For free dispersion, the bubbles were sufficiently far from the wall that the surrounding fluid could be approximated as the free stream speed. The mean relative velocity of the sliding bubbles was computed by subtracting the average streamwise velocity of the fluid for the mean bubble transverse position. In general, all the measured bubble relative velocities were bounded by the empirical rise velocity distributions of Clift et al. (1978) for clean and contaminated conditions as a function of bubble diameter.

As can be observed from Table 2, the bouncing bubble type of trajectory was limited to bubbles with $d_B > 0.8$ mm. Fig. 18 compares the before ($V_{B,in}$) and after ($V_{B,out}$) bouncing velocities for bubbles between 0.8 and 1.2 mm in diameter. Notably, the ratio of the incoming bubble, transverse velocities are quite high, e.g. of the order of eight times the peak of the rms of the liquid transverse fluctuating velocity, thus indicating lift forces dominate this motion (Felton and Loth, 2001). From this figure one may also note the ratio of incoming velocity to outgoing velocity approximates the coefficient of restitution. The decrease in this ratio as bubble size decreases suggests that the smaller bubbles lose more energy. When considering the incoming velocity and associated transverse Reynolds number, this trend is qualitatively consistent with a recent experiment by Zenit et al. (1999) for solid particles rebounding in water, who attributed the trend to increased viscous effects.

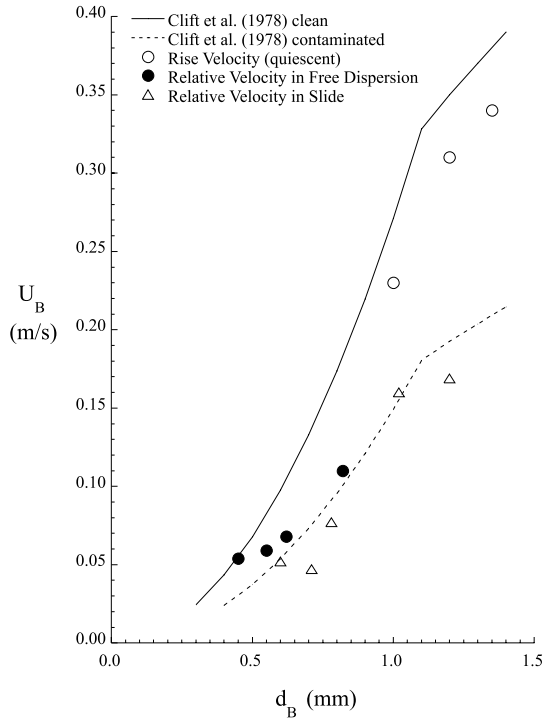

Fig. 17. Comparison of the relative slide, free dispersion, and theoretical and experimental terminal velocities for 0.4–1.5 mm diameters bubbles.

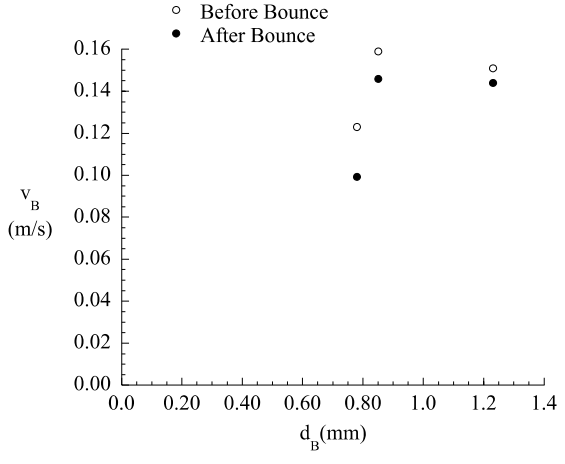

Fig. 18. Comparison of (a) incoming and rebounding bounce velocities after the first bounce and (b) incoming bounce velocity to maximum fluctuating velocity ratio versus Stokes number.

4. Conclusions

A vertical turbulent boundary layer in a water tunnel was employed to investigate distribution and motion of a dilute suspension of spherical bubbles. The test conditions included a filtered tap-water flow with $Re_\delta = 13{,}000$–$20{,}000$ and bubbles with $Re_B = 10$–120. Inspection of the void fraction profiles yielded four distinct distribution shapes, generally including all bubbles trapped along the wall (Type I profile) to all bubbles distributed in the boundary layer (Type II profiles). The trapping phenomenon of the Type I profiles occurred at the higher Stokes number (and drift parameter) conditions associated with the large diameter spherical bubbles. It was primarily associated with specific turbulent events which quickly moved a bubble toward the wall, after which it bounced a few times, and could be retained along the wall in a sliding motion by the lift force. Lower Stokes number conditions at the same injection location resulted in the bubbles behaving nearly as passive scalars and diffusing throughout the boundary layer. The resulting peak void fraction transverse location for such bubbles was consistent with the upstream injection point. This indicates a lack of a substantial mean drift for bubbles not very close to the wall. In some cases, a single injection point and bubble size could result in a combination of these two near-wall and free-dispersion distributions (termed Type II profiles). And in addition, bubbles distributions could also be maintained at the boundary layer edge (Type IV profiles).

In general, three types of bubble trajectories were observed in the boundary layer: sliding bubbles, bouncing bubbles, and free dispersing bubbles. For all three trajectories, the relative velocities of the bubbles with respect to the surrounding fluid as a function of bubble diameter were similar to rise velocities found in quiescent flow. The sliding bubbles maintained a transverse location of about 2/3 of a diameter from the wall for all bubble sizes, similar to previous results for ellipsoidal bubbles. The bouncing bubbles exhibited a coefficient of restitution which decreased with bubble diameter, qualitatively similar to previous solid particle experiments. For free dispersion bubbles, the void fraction diffusion rates were qualitatively similar to that expected from solid particle diffusion as a function of drift parameter. In summary, both free-dispersion and wall-interaction physics can be essential to bubble distributions in wall-bounded flows.

Acknowledgements

This work was supported by the Office of Naval Research under grant N00014-96-1-0312. Mr. Anthony Flores also provided valuable experimental assistance.

References

Beyerlein, S.W., Cosman, R.K., Ritcher, H.J., 1985. Prediction of bubble concentration profiles in two-phase flow. Int. J. Multiphase Flow 11 (5), 629–641.

Bocksell, T.L., Loth, E., 1999. A CRW Model for Diffusion of Bubbles and Particles. ASME Summer Fluids Engr. Meeting, San Fransisco, FEDM98-7366.

Braslow, A.L., Hicks, R.M., Harris, R.V., 1966. Use of grit-type boundary layer-transition trips. NASA SP-124.

Clift, R., Grace, J.R., Weber, M.E., 1978. Bubbles, Drops and Particles. Academic Press, New York.
Felton, K., 1999. A study of spherical bubbles in a vertical turbulent boundary layer. Ph.D. Thesis, Department of Aeronautical & Astronautical Engineering, University of Illinois at Urbana-Champaign, IL.
Felton, K., Loth, E., 2001. Spherical bubble motion in a turbulent boundary layer, Physics of Fluids (Sept. 2001).
Ford, B., Loth, E., 1998. Forces on ellipsoidal bubbles in a turbulent free shear layer. Phys. Fluids 10, 178–188.
Ford, B., Loth, E., 2000. Diffusion of ellipsoidal bubbles in a turbulent shear layer. Int. J. Multiphase Flow 26, 503–516.
Klebanoff, P.S., 1954. Natl. Advisory Comm. Aeronauti. Tech. Notes No. 3178.
Lance, M., Bataille, J., 1991. Turbulence in the liquid phase of a uniform bubbly air–water flow. J. Fluid Mech. 222, 95–118.
Lasheras, J., 1998. University of California at San Diego, personal communication.
Liu, T.J., 1993. Bubble size and entrance length effects on void development in a vertical channel. Int. J. Multiphase Flow 19, 99–113.
Loth, E., 1998. An Eulerian model for turbulent diffusion of particles in free shear layers. AIAA J. 36 (1), 12–17.
Loth, E., 2000. Numerical approaches for motion of dispersed bubbles, particles and droplets. Prog. Energy Combust. Syst. 26 (3), 161–223.
Marie, J.L., Moursali, E., Tran-Cong, S., 1997. Similarity law and turbulence intensity profiles in a bubbly boundary layer at low void fractions. Int. J. Multiphase Flow 23 (2), 227–247.
Meinhart, C.D., 1994. Investigation of turbulent boundary-layer structure using particle imaging velocimetry. Ph.D. Thesis, Department of Theoretical and Applied Mechanics, University of Illinois.
Merkle, C., Deutsch, S., 1992. Microbubble drag reduction in liquid turbulent boundary layers. Appl. Mech. Rev. 45, 103–127.
Michiyosi, I., Serizawa, A., Takashi, O., Gakuhari, K., Ida, T., 1986. Heat transfer and hydraulics of liquid metal-gas two phase magneto-hydrodynamic flow. In: Proceedings of the 8th International Heat Transfer Conference, San Francisco, CA.
Moursali, E., Marie, J.L., Bataille, J., 1995. An upward turbulent bubbly boundary layer along a vertical flat plate. Int. J. Multiphase Flow 21, 107–117.
Nakoryakov, V.E., Kashinsky, O.N., Burdukov, A.P., Odnoral, V.P., 1981. Local characteristics of upward gas–liquid flows. Int. J. Multiphase Flow 7 (1), 63–81.
Oguz, H.N., Prosperetti, A., 1993. Dynamics of bubble growth and detachment from a needle. J. Fluid Mech. 257, 111–145.
Park, W.C., Klausner, J.F., Mei, R., 1995. Unsteady forces on spherical bubbles. Exp. Fluids 19, 167–172.
Poorte, R.E.G., 1998. On the motion of bubbles in active grid generated flows. Ph.D. Thesis, Universite of Twente, Netherlands, September.
Reeks, M., 1977. On the dispersion of small particles suspended in an isotropic turbulent fluid. J. Fluid Mech. 83 (Part 3), 529–546.
Sekoguchi, K., Fukui, H., Sato, Y., 1981. Flow characteristics and heat transfer in vertical bubble flow. In: Bergles, A.E., Seikan, I. (Eds.), Two-Phase Flow Dynamics. Kobe, Japan, pp. 59–74.
Sene, K.J., Hunt, J.C.R., Thomas, N.H., 1994. .The role of coherent structures in bubble transport by turbulent shear flows. J. Fluid Mech. 259, 219–240.
Serizawa, A., Kataoka, I., Michiyosi, I., 1975. Turbulence structure of air–water bubbly flows: Part I–III. Int. J. Multiphase Flow 21 (3), 221–259.
Shridar, G., Katz, J., 1995. Drag and lift forces on microscopic bubbles entrained by a vortex. Phys. Fluids 7, 389–399.
Stock, D.E., 1996. Particle dispersion in flowing gases. ASME J. Fluids Eng. 188, 4–17.
Tio, K.-K., Liñán, A., Lasheras, J.C., Gañán-Calvo, A.M., 1993. The dynamics of bubbles in periodic vortex flows. Appl. Sci. Res. 51, 285–290.
Tomkins, C., 1997. A particle image velocimetry study of coherent structures in a turbulent boundary layer. M.S. Thesis, Department of Theoretical and Applied Mechanics, University of Illinois at Urbana–Champaign, IL.
Tran-Cong, S., Marie, J.L., Perkins, R.J., 1997. Experimental study of the bubble dispersion in a turbulent boundary layer. ASME Fluids Engineering Division Summer Meeting, Vancouver, B.C.
van der Welle, R., 1985. Void fraction, bubble velocity and bubble size in two-phase flow. Int. J. Multiphase Flow 11 (3), 317–345.

Wang, S.K., Lee, S.J., Jones, O.C., Lahey, R.T., 1987. 3-D Turbulence structure and phase distribution measurements in bubbly two-phase flows. Int. J. Multiphase Flow 13 (3), 327–343.

Young, J.B., Hanratty, T.J., 1991. Trapping of solid particles at a wall in a turbulent flow. AIChE J. 37 (10), 1529–1536.

Zenit, R., Joseph, G., Hunt, M., 1999. The coefficient of restitution for liquid immersed collisions. ASME Summer Fluids Engineering Meeting, FEDSM99-7793, San Francisco, July.